Grant Agreement No.: 955413

Project acronym: ENGIMMONIA

Project title: Sustainable technologies for future long distance shipping towards complete decarbonisation

Call (part) identifier: H2020-EU.3.4. - Smart, Green And Integrated Transport

Thematic Priority: LC-MG-1-13-2020 - Decarbonising long distance shipping

Starting date of project: 1st May, 2021

Duration: 48 months

WP2 – "Ammonia combustion and emission modelling"
D2.3 – "Tabulated chemistry coupled with CFD for combustion modelling"

Due date of deliverable
30-04-2024
Actual submission date
30-04-2024

Deliverable version
1.0

Organisation name of lead contractor for this deliverable: ###

Dissemination Level		
CO	Confidential	
PU	Public	X

Executive Summary

This deliverable D2.3 corresponds to Task 2.3, where Lund University develops and validates a "tabulated chemistry coupled with CFD for combustion modeling." The CFD model aims to simulate ammonia/diesel dual-fuel combustion in marine engines, utilizing the chemical kinetic mechanisms developed in Task 2.1. These mechanisms are validated for ammonia at high pressure and high temperature, with the objective of achieving reduced computational costs.

The integration of detailed chemical kinetics, containing more than 1000 species and several thousand reactions, into flow simulations in a CFD code is computationally unfeasible for engine design simulations, requiring significant memory and CPU time. Consequently, tabulation methods such as the flamelet generated manifold (FGM) model have garnered attention. While FGM models have been developed and applied in single-fuel compression-ignition engine simulations, they have not been adapted for dual-fuel engines. In Task 2.3, a dual-fuel FGM model is developed.

A key feature of the new FGM model is the creation of a one-dimensional dual-fuel counterflow combustion configuration that emulates the flamelet manifolds in dual-fuel engine combustion. The FGM model is validated against direct numerical simulation (DNS) results, achieving satisfactory agreement between the DNS and FGM results. Notably, the computational time for the FGM is 1/160th of that required for DNS.

The integration of a reduced chemical kinetic mechanism, typically comprising fewer than 100 species and a few hundred reactions, is commonly employed in CFD engine combustion simulations. While this approach is computationally feasible, achieving significant computational efficiency is crucial for engine design simulations.

In Task 2.3, a chemistry coordinate mapping (CCM) approach is developed to enhance computational efficiency. CCM involves the direct integration of the chemical kinetic mechanism into flow simulations, with the time-consuming integration of chemical reaction rates—requiring a stiff solver and multiple fractional time steps—performed within CCM phase space cells. The integrated reaction rates are mapped to physical space cells. As each phase-space cell corresponds to multiple physical space cells, the integration of reaction rates is conducted only once for multiple physical space cells.

The CCM method is applied to two dual-fuel engines, and the results are compared with those obtained from the direct integration (DI) of chemical reaction rates in physical space. The comparison demonstrates good agreement between the CCM results and the DI results, while reducing computational time by two-thirds.

Table of Contents

List of Figures

No table of figures entries found.

Abbreviations and acronyms

RCCI	Reactivity controlled compression-ignition
DDFS	Double direct fuel stratification
FGM	Flamelet generated manifold
CCM	Chemistry coordinate mapping
CFD	Computational fluid dynamics
DNS	Direct numerical simulation
RANS	Reynolds averaged Navier-Stokes
FGM	Flamelet generated manifolds

1. Introduction

This deliverable was prepared within the framework of Work Package 2, Task 2.3, "Tabulated chemistry coupled with CFD for combustion modelling". The work is carried out at Lund University, Department of Energy Sciences. The work aims to develop computationally efficient CFD models for design simulations of ammonia marine engine combustion and emission process. Two approaches are developed in Task 2.3: (a) flamelet-generated manifold (FGM) modeling of ammonia/diesel combustion using detailed chemical kinetic mechanisms containing thousands of species and elementary reactions; (b) chemistry coordinate mapping (CCM) approach for reduced chemical kinetic mechanisms containing fewer than 100 species and a few hundred elementary reactions.

Ammonia is recognized as one of the most promising carbon-free fuels for future marine engines. However, utilizing pure ammonia in engines presents several challenges, including low flame speed, a narrow flammability range, and difficulties in ignition. To address these challenges, two novel engine concepts have been investigated both in academic and industrial research: one is the Reactivity-Controlled Compression Ignition (RCCI) [1–3], and the other is the Direct Dual Fuel Stratification (DDFS) [4]. In ammonia RCCI engines, a small quantity of diesel is injected into the cylinder to ignite the premixed ammonia/air mixture. Ideally, only a very small amount of diesel (e.g., < 10%) is preferred to achieve high combustion efficiency and minimize emissions of NO and N2O, a greenhouse gas with a global warming potential (GWP) 300 times that of CO2 [5]. However, recent engine experiments have indicated that a minimum of 20–30% diesel energy share is required to attain high combustion efficiency without significant ammonia slip [2, 6]. The DDFS engine concept utilizes dual high-pressure common rail systems to separately inject liquid ammonia and diesel fuel into the engine cylinder. Ensuring optimal engine performance across various combustion regimes relies on accurately controlling several factors, such as the energy ratio between ammonia and diesel, injection angles, and the coordinated timing of fuel injections.

High-fidelity computational fluid dynamics (CFD) simulations play a crucial role in further developing and optimizing RCCI engines [2, 7]. These simulations have revealed that RCCI combustion involves multiple combustion modes [8–10], including auto-ignition of the high-reactivity fuel, ignition wave propagation in the mixing layer of high and low-reactivity fuels, premixed flame propagation in the low-reactivity premixed fuels, and diffusion flame to burn out the fuel-rich intermediate fuel with the oxygen in the postflame zone of the premixed flame. This complex combustion process is simulated by directly coupling finite-rate chemistry [2, 11]. However, the direct coupling of finite-rate chemistry in CFD simulations can be computationally demanding, especially considering the number of species and reactions in the chemical kinetic model. Consequently, it is desirable to develop high-efficiency combustion models for CFD simulations of RCCI engine combustion.

For conventional compression-ignition engine CFD simulations, researchers have developed and utilized flamelet-generated manifolds (FGM) models [12–15]. In these models, thermodynamic variables like species mass fractions and temperature are represented based on a few principal variables [16]. Although this representation isn't analytical, a numerical solution of the transport equations in a low-dimensional configuration generates a numerical representation of the FGM function—a process known as FGM tabulation. The transport equations for the principal variables are solved, with their source terms expressed as functions of these variables. Mass fractions and temperature are then derived from the FGM tabulation. This approach allows CFD simulations to focus solely on solving transport equations for the principal variables, making computations much more efficient and independent of the chemical kinetic mechanisms' size.

The main challenge in FGM models lies in generating the FGM function, known as FGM tabulation. In conventional compression-ignition engine simulations, the governing equations of the chemical reactive flow system are often solved in a one-dimensional counterflow configuration (1D-CC) during the tabulation process [12, 13, 17]. In this process, FGM principal variables, such as the mixture fraction and a carefully selected reaction progress variable (RPV), are chosen to represent the reaction states. For fuels with multiple components, two or more FGM principal variables have been utilized [14, 18]. However, FGM modeling of RCCI engines has not been addressed in the literature. Using the 1D-CC approach to generate the FGM function for RCCI engine combustion is inappropriate because the 1D-CC solution does not encompass all combustion modes present in RCCI combustion.

In Section 2, a novel approach is introduced for FGM tabulation specifically tailored for ammonia RCCI engine combustion. A 1D RCCI configuration (1D-RC) is proposed to facilitate the generation of the FGM function. The effectiveness of the FGM tabulation is assessed through direct numerical simulations (DNS) data in an a priori lookup test. Subsequently, the FGM model is integrated into a DNS setup to reproduce the RCCI combustion process. The obtained results are then compared with DNS results obtained through direct coupling of the chemical kinetic mechanism. Remarkably, the FGM-DNS approach demonstrated a significant speedup rate of 160 times during the simulation compared to DNS with direct chemistry coupling in this study. Additionally, the FGM-DNS method accurately captures the fine structures of the reaction zones.

Despite the promising potential of the DDFS concept, it faces notable technical hurdles, particularly regarding the high-pressure injection of ammonia. Challenges such as material corrosion and the need for precise control of the injection process present significant obstacles. Zhang et al. [4] conducted comprehensive experiments on a laboratory-scale marine engine, thoroughly examining the impacts of different parameters and emphasizing the crucial role of finely adjusting diesel injection timing to achieve successful ignition of the liquid-phase ammonia spray, thereby effectively mitigating NOx emissions.

CFD simulations of DDFS engines offer a chance to fine-tune the injection process of diesel and ammonia. Finite-rate chemistry models, utilizing reduced chemical kinetic mechanisms, are frequently utilized to replicate the various combustion modes present in DDFS combustion, encompassing ignition initiation, premixed and diffusion flames, as well as the interaction between turbulence and chemical reactions. To optimize computational efficiency, a chemistry coordinate mapping (CCM) approach has been devised. Section 3 introduces this method, showcasing its application in simulations of ammonia/diesel DDFS combustion, and assessing both accuracy and computational efficiency.

2. FGM model for ammonia/diesel RCCI engine simulation

2.1. FGM tabulation strategy

Figure 1 illustrates two low-dimensional configurations that generate FGM tabulation: 1D-CC and 1D-RC. Two distinct streams are identified in both scenarios: Stream B for the premixed ammonia/air mixture stream and Stream F for the n-heptane/ammonia/air mixture stream. The mixing of these streams is quantified by the mixture fraction (Z) calculated with normalized carbon element mass fractions (Y_C). Z is defined in Eq. (1). In this context, the subscripts B and F correspond to streams B and F, respectively.

$$Z = (Y_C - Y_{C,B})/(Y_{C,F} - Y_{C,B}) \tag{1}$$

The distinction between the two configurations primarily lies in their respective Z distributions. In the case of 1D-CC depicted in Fig.1a, the left boundary at x = 0 mm supplies Stream B, while the right boundary (at x = 20 mm in this instance) supplies Stream F. This setup results in a spatially monotonically increasing Z distribution, ranging from 0 for pure Stream B at the left boundary to 1 at the right boundary for pure Stream F. Notably, the extreme values of Z are confined exclusively to the boundaries rather than the inner domain. Conversely, in the 1D-RC configuration shown in Fig.1b, Stream F is embedded in the center of Stream A. This configuration yields a Z distribution that can be approximated by the hyperbolic tangent function [9]. Unlike the 1D-CC configuration, the 1D-RC configuration encompasses a substantial region with Z = 0. The thickness of the mixing layer is 0.4δ with the value of Z ranging from 0.02 to 0.98. This thickness governs the gradient of the mixing layer and, consequently, the scalar dissipation rate (SDR), expressed as $\chi = 2D\nabla Z \cdot \nabla Z$, where D represents mass diffusivity.
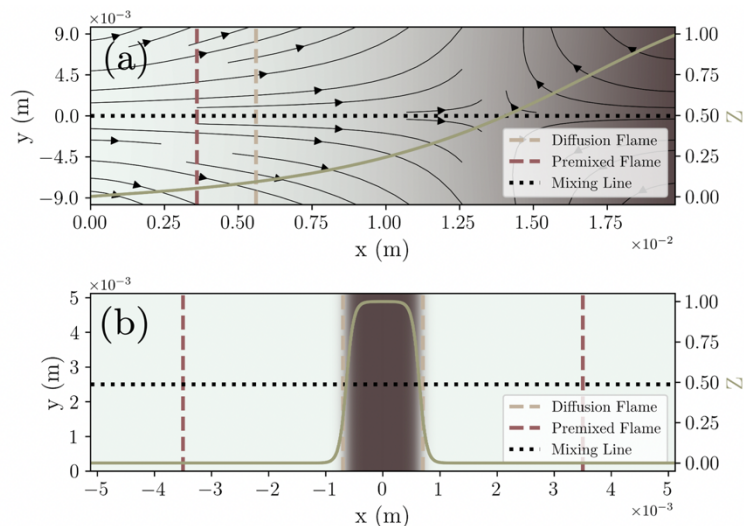

Fig. 1: Low-dimensional configurations used to generate FGM tables. (a) One-dimensional counter-flow configuration (1D-CC), and (b) one-dimensional RCCI configuration (1D-RC). The background is colored by the mixture fraction, whose distribution is also marked with gray lines. The location of the diffusion flame and premixed flame are marked with gray/brown dashed lines, respectively.

In RCCI engines, the emergence of a freely propagating premixed flame into the background (i.e., Stream B) becomes possible if Stream B is a premixed fuel/air mixture. The Z distribution in the 1D-RC configuration facilitates such flame propagation, as illustrated by a representative 1D simulation conducted within this domain, shown in Fig.2a. The detailed operating conditions are outlined in Table 1. The simulation results indicate that ignition occurs in the mixing layer at t=0.89 ms. Subsequently, two reaction fronts, identified by regions with high-temperature gradients, propagate towards the fuel-rich center region around x=0 and the premixed ammonia/air mixture (x > 1 mm), respectively. By adopting a RPV denoted as c and following Eq. (2) [19], and mapping the results to the $Z - c$ space, it is observed that the flame can sweep the $Z - c$ space after 3.2 ms, propagating to regions with $Z = 0$. Furthermore, the theoretically maximum c in the premixed ammonia/air mixture, calculated from a complete transformation from reactants to products, can be reached in this case at 3.2 ms.

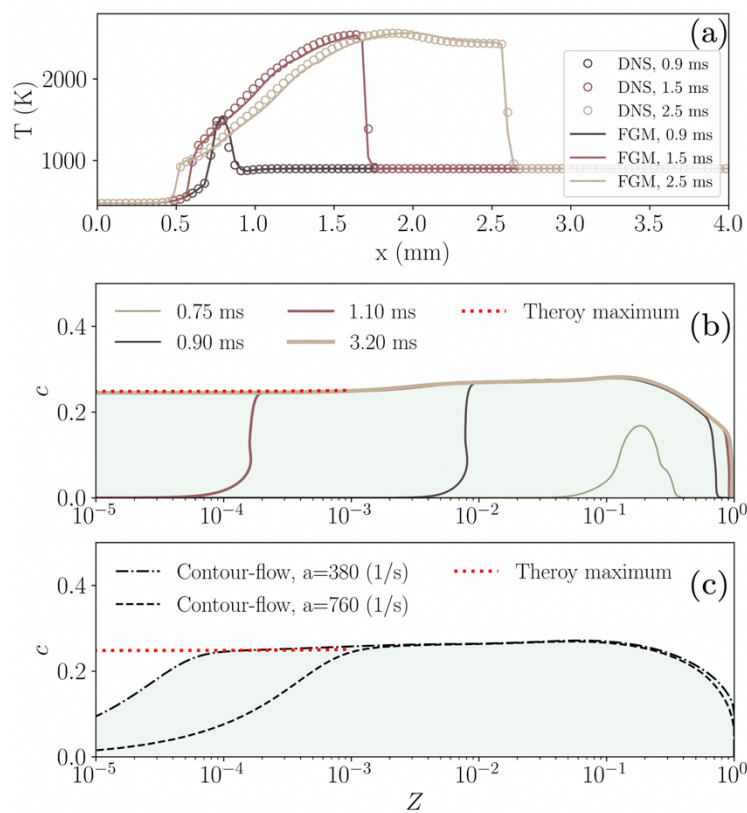$$c = 1.2Y_{CO2} + 0.9_{YCO} + 2.7Y_{HO2} + 1.5Y_{CH2O} + 1.2Y_{H2O} \tag{2}$$

Fig. 2: FGM table properties: (a) temporal evolution of temperature distribution in the 1D-RC physical domain; (b) distributions of c in the 1D-RC Z coordinate for several selected time steps (c) distributions of steady c in the 1D-CC physical domain. The shadow region indicates the domain that c can reach.

In contrast, for the 1D-CC solution shown in Fig. 2c, the theoretical maximum c cannot be reached due to the limitations inherent in the 1D-CC. The position of the premixed flame cannot freely propagate to the pure Stream B, which exists only at the boundary, as previously mentioned, owing to the imposed inflow boundary condition. While decreasing the inflow velocity (and hence the strain rate) would allow the flame to be closer to the inflow, the imposed inflow temperature serves as a heat loss source, impacting the reaction zone temperature and reaction rate. As a consequence, the simulation using 1D-CC struggles to include freely propagating premixed flame, as the premixed flame cannot easily extend to the pure Stream B. In contrast, the 1D-RC domain proves more applicable, accommodating all combustion modes,

including premixed flame propagation in the later stages of RCCI combustion. Hence, it is recommended for FGM tabulation in the context of RCCI combustion.

Table 1: Operating conditions.

Parameters	Stream F	Stream B
Z	1	0
p (bar)	59	59
T (K)	475	900
$Y_{C_7H_{16}}$ (%)	50.0	0.0
Y_{NH_3} (%)	6.5	13.0
Y_{N_2} (%)	33.3	66.6
Y_{N_2} (%)	10.2	20.4
ϕ	18	0.9

2.2. Governing equations and numerical method

The transport equations for Z and c are provided in Eq. (3), where D represents mass diffusivity, and Sc denotes the rate of c. These equations are derived under the assumption of unity Lewis numbers for all species, in accordance with the literature on FGM modeling [20, 21]. The value of D is computed from the kinematic viscosity ν, assuming a Schmidt number Sc = ν/D of 0.7.

$$\frac{\partial \rho Z}{\partial t} + \frac{\partial \rho u_j Z}{\partial x_j} = \frac{\partial}{\partial x_j}\left(\rho D \frac{\partial Z}{\partial x_j}\right)$$

$$\frac{\partial \rho c}{\partial t} + \frac{\partial \rho u_j c}{\partial x_j} = \frac{\partial}{\partial x_j}\left(\rho D \frac{\partial c}{\partial x_j}\right) + S_c$$

(3)

The thermodynamic variables (T, Y_i, ν) are tabulated as functions of Z and c based on the 1D-RC solution, while the CFD simulation will only transport Z, c, along with the continuity and momentum equations. Temperature and species information will be retrieved during the post-processing from the tabulated FGM function.

DNS of ammonia/n-heptane dual-fuel RCCI combustion in a two-dimensional (2D) domain was conducted to validate the FGM model. The 2D DNS results encompass all necessary combustion modes in a three-dimensional engine cylinder, although the turbulence in 2D lacks the mechanisms of stretching and cascading. The DNS solver, named reactingDNS [21, 22], operates on the OpenFOAM-10 platform and utilizes mixture-averaged transport properties to account for differential diffusion. The transport equations are discretized employing second-order temporal and fourth-order spatial discretization schemes.

For tabulation purposes, a customized adaptive solver, denoted as tReactingDNS, is employed to generate FGM tabulation from a 1D-RC domain, incorporating an adaptive data writeout interval. A skeletal ammonia/n-heptane reaction mechanism [23], comprising 69 species and 389 reactions, is utilized to model the chemical reactions of ammonia and n-heptane. This mechanism is applied in both the 1D tabulation simulation and the 2D DNS with full chemistry. DNS is carried out using the FGM model, where the transport equations (3) are solved instead of the species mass fraction and energy equations. This simulation is referred to as FGM-DNS.

Figure 3 illustrates the computational domain with dimensions of 20.48 mm in length and 5.12 mm in width. In this domain, Stream B is premixed ammonia/air, located in the Premixed (PM) region, as shown in Figure 3. The pilot fuel, n-heptane in this case, is injected into the PM region at the center with an adjustable velocity u, resulting in mixing between the pilot fuel and

Stream B. The mass fraction of n-heptane is 0.5 in Stream F. Thermochemical conditions for both streams are detailed in Table 1.
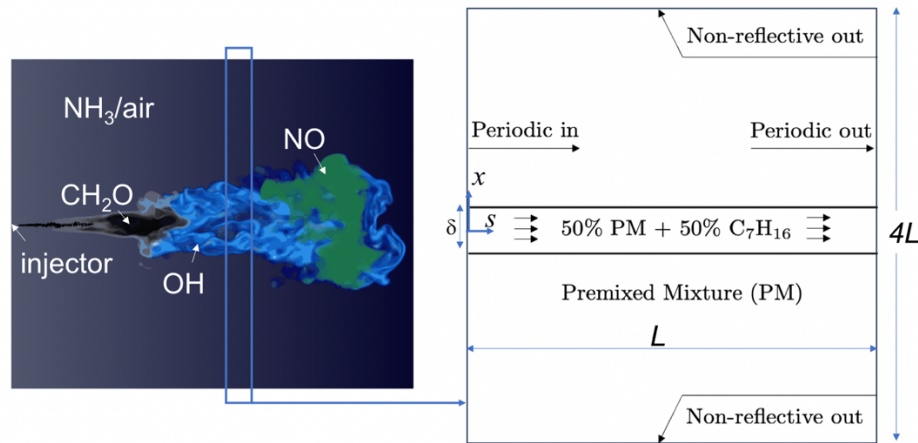

Fig. 3: A schematic of the computational domain. The domain is taken from a downstream region of the n-heptane jet into a premixed ammonia/air mixture.

The evaporation of n-heptane is considered through the adiabatic mixing of gasified pilot fuel with Stream B before the start of the DNS, following recommendations in Ref. [24]. The initial species fields are calculated using $Y_i = ZY_{F,i}+(1-Z)Y_{B,i}$, where i encompasses all involved species, such as C7H16, NH3, N2, O2. The initial temperature is determined using a fitted function of Z with respect to T, obtained from one-dimensional mixing between the two streams. All the aforementioned parameters are relevant to the conditions around the top-dead-center of an ammonia/n-heptane RCCI engine [2].

Two cases are configured in the present study. The only difference between them is the applied jet velocity. No jet velocity is applied for Case 1, while a jet velocity at 10 m/s is used for Case 2. A background turbulent velocity field is superimposed onto an initial turbulent flow field generated using a solver described in Ref. [25] with a prescribed energy spectrum, assuming an integral velocity u′=1.1 m/s and integral length l_0=2.5 mm. The 1D-RC domain used to generate the FGM tabulation is similar to the 2D DNS domain; however, the streamwise direction s is neglected. Mesh-sensitive analysis has been carried out in the numerical simulations in the 1D-RC domain to examine the required mesh resolution. A mesh size of 5 μm yields grid independent results. The same grid in the stream76 wise and spanwise directions is used, with results in 4096×1024 cells.

2.3. Results and discussion

Figure 4 compares the FGM-based DNS results and the original DNS results. The temporal evolution of the temperature field shows the ignition process and subsequent flame propagation. In Case 1, ignition occurs at 0.9 ms in the mixing layer between the low-temperature n-heptane/ammonia/air region (white color) and the high-temperature premixed ammonia/air region (light brown). The mixing layer is slightly wrinkled by the background turbulence imposed as the initial condition. At 1.2 ms, the entire mixing layer is ignited, and the wrinkle scale in the reaction zone increases with time. After that, the high-temperature region broadens in the spanwise direction. The local heat release rate field at 3 ms shows three reaction layers: the outer layer corresponds to the premixed flame propagation outward toward the premixed ammonia/air mixture, consuming the ammonia (cf. the NH3 distribution at 3 ms); an inner

premixed flame propagates inward in the premixed n-heptane/ammonia/air mixture in the center of the domain consuming n-heptane (cf. C7H16 distribution at 3 ms). In between the two reaction layers is a diffusion flame where the fuel-lean oxidizer mixtures oxidize the fuel-rich combustion intermediate species. This reaction zone structure predicted using the FGM-based DNS agrees perfectly with the full DNS results. Only a minor difference in the diffusion flame layer between the DNS and FGM-DNS can be observed. The NO and N2O distributions from the FGM-DNS are also in very good agreement with the DNS results.
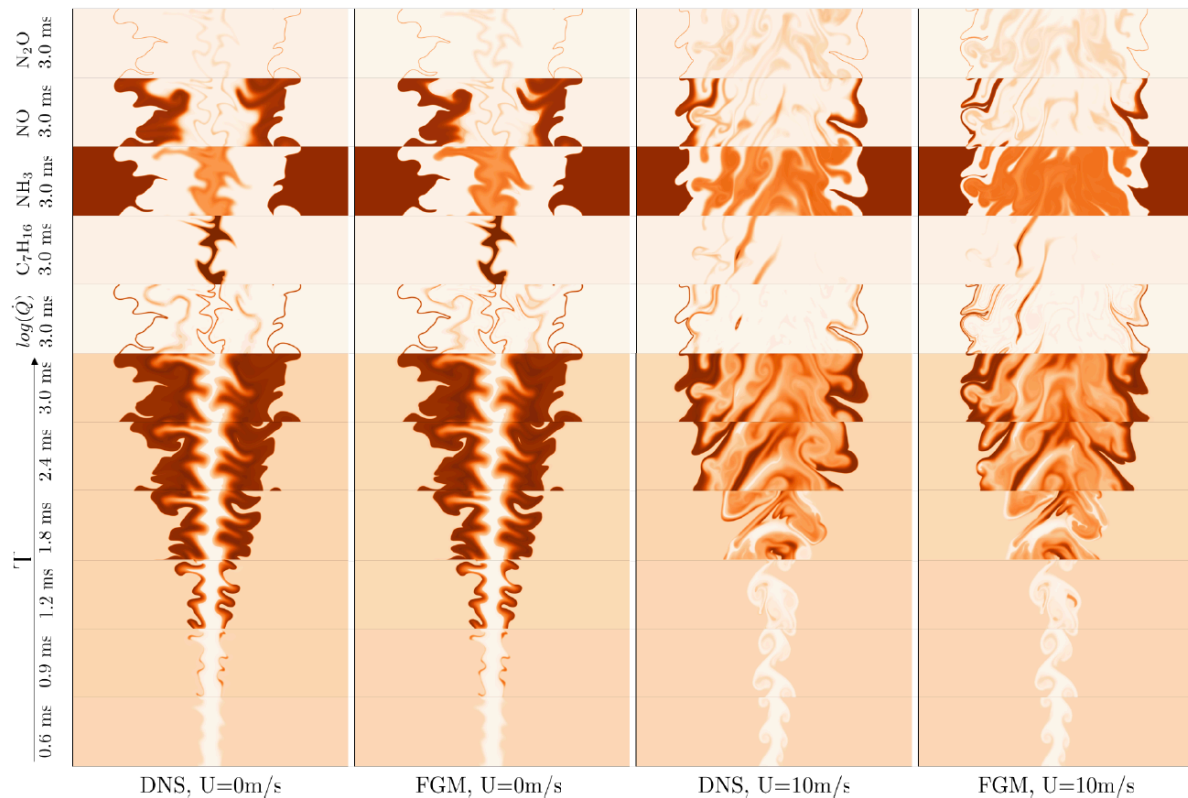

Fig. 4: Temporal and spatial evolution of temperature field from 0.9 ms to 3 ms, and spatial distribution of local heat release rate Q (in log-scale), mass fractions of n-heptane, ammonia, NO and N2O. Light color: low values; dark color: high values.

In Case 2, the center n-heptane/ammonia/air region is imposed with a mean velocity of 10 m/s. The mean velocity gradient in the mixing layer enhances the formation of turbulence, significantly impacting the ignition and flame propagation. It is shown that the onset of ignition in the mixing layer is delayed to 1.2 ms. Despite later ignition, the outer premixed flame propagates at a higher speed than Case 1, as indicated in the distributions of the local heat release rate and unburned ammonia. Owing to the stronger turbulent diffusion, in the center region of the domain, n-heptane is nearly completely burned, and the inner premixed flame front no longer exists at 3 ms. The faster mixing of the n-heptane/ammonia/air region with the premixed ammonia/air region pushes the diffusion flame closer to the outer premixed flame, which results in a smaller region with high flame temperature and high NO mass fraction. In the inner fuel-rich region, a substantial amount of ammonia is left unburned, resulting in lower NO but higher N2O. FGM-DNS successfully captures the main structures of the reaction zones and the distributions of species and temperature in Case 2.
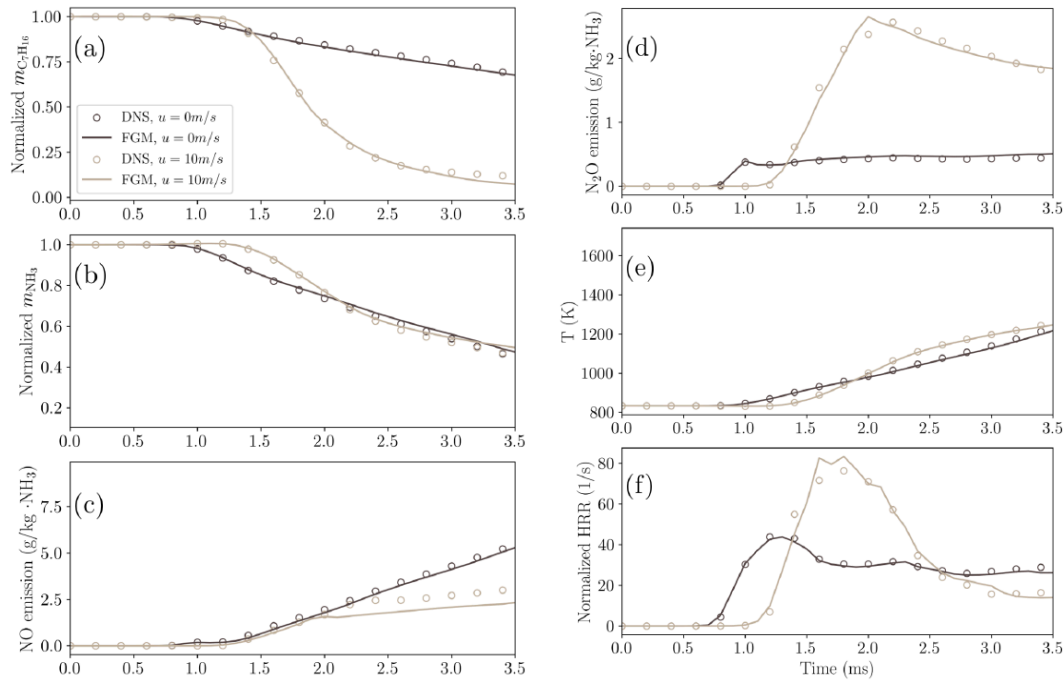
Fig. 5: Integral overall statistics, including normalized mass of (a) C7H16, (b) NH3, (c) NO, (d) N2O in the domain, as well as (e) mass weighted temperature T and (f) normalized heat release rate in the domain. The fuels are normalized by their initial value, while the emissions are normalized with the initial mass of NH3. The heat release rate is normalized with the total energy at the initial time.

The temporal evolution of the total mass of fuels (NH3 and C7H16) shows the impact of jet velocity on the fuel consumption process, Fig. 5(a,b). The jet-induced turbulence significantly accelerated the combustion of the n-heptane in Case 2 due to faster turbulent diffusion and mixing. At the same time, it had a minor impact on the combustion of ammonia since the combustion occurs mainly in the outer premixed flame, which is further away from the mixing layer; hence, the impact of turbulence is smaller there. The results from FGM-DNS agree fairly well with the DNS results in both cases. From the heat release rate, it is clear that jet-induced turbulence postponed the ignition but promoted the combustion rate after the ignition at first.

In the later stage, i.e., after 3 ms, the low jet velocity case (Case 1) has a higher heat release rate because of the continuous combustion of the C7H16 in the center region. While for Case 2, C7H16 is almost consumed. The mean temperature is thus higher in the later stage in Case 1. The mean temperature in the domain and the total heat release rate from FGM-DNS agree well with the DNS results. Figures 5c and d show that jet-induced turbulence impacts the NO and N2O emissions. Case 2 has a lower NO emission but higher N2O emission than Case 1. From the spatial distribution of NO and N2O in Fig. 4, it is clear that this is due to the change of flame structures. The fast mixing of unburned ammonia to the high NO region close to the outer premixed flame consumed NO in Case 2. On the other hand, N2O is seen in the reaction zone of ammonia. Thus, a distributed ammonia reaction zone in the center region in Case 2 resulted in a high and distributed N2O formation. This process is well captured in the FGM-DNS.

The comparison between the FGM-DNS and DNS results presented above is excellent in Case 1, while in Case 2 there are certain minor discrepancies between the results. This is attributed to the flamelet assumption, which, while still applicable, is not perfectly valid in this particular

scenario. The use of unity Lewis number in the FGM and the choice of RPV may contribute to the deviations from the DNS where differential diffusion is accounted for. Further optimization of these aspects could enhance the accuracy of FGM predictions.

Table 2: CPU time required for a CFD time step.

Method	DNS	FGM	Speedup ratio
CPU time (s)	52.5	0.33	160

The most promising aspect of FGM lies in its high efficiency. Table 2 shows a comparison of the CPU time required for the simulation of a single time step for Case 2 at 2 ms. Remarkably, the FGM method completed the simulation in just 0.33 seconds, whereas the DNS method required 52.5 seconds. This translates to an impressive acceleration ratio of approximately 160. If a more comprehensive and larger chemical mechanism is employed, an even higher acceleration ratio is anticipated, given that FGM does not directly solve the chemistry during simulations.

The work has been accepted for oral presentation at the 40th International Combustion Symposium to be held in Milan, Italy, July 2024. The paper details are:

YC Zhou, S Xu, L Xu, XS Bai, FGM modeling of ammonia/n-heptane combustion under RCCI engine conditions, 40th International Combustion Symposium, accepted for oral presentation.

3. CCM modeling for ammonia/diesel dual-fuel engine simulation

3.1. CCM approach and phase space principal variables

In combustion simulations employing finite-rate chemistry, solving the species transport equation is the most time-consuming task. The computation time scales linearly with the number of species in the chemical kinetic mechanism. The transport equations are typically solved in two fractional steps. In Step 1, the chemical reaction rates are integrated from time t_n to $t_n+\Delta t$,

$$(\rho Y_k)^* = (\rho Y_k)^n + \int_{t_n}^{t_n+\Delta t} \dot{\omega}_k dt$$

where Δt is a time step. The integration requires multiple fractional time steps and a stiff solver, making it the most time-consuming step. In Step 2, the convective and diffusive transport terms are integrated as follows,

$$\frac{(\rho Y_k)^{n+1} - (\rho Y_k)^*}{\Delta t} + \frac{\partial \rho u_j Y_k}{\partial x_j} = \frac{\partial}{\partial x_j}\left(-\rho Y_k V_{k,j}\right), \quad (k = 1, \ldots, N),$$

The Chemistry Coordinate Mapping (CCM) approach was developed to expedite the numerical simulation of turbulent reactive flows by directly integrating the chemical reactions [26, 27]. As depicted in Fig. 6, within a combustion field, numerous points in physical space share identical thermodynamic variables such as temperature and species mass fractions, resulting in identical chemical reaction rates. The fundamental concept of CCM involves grouping computational cells in physical space that has similar thermal dynamic properties into a phase space zone and integrating the chemical reaction rates within this zone. These rates are then mapped back to multiple physical space cells.
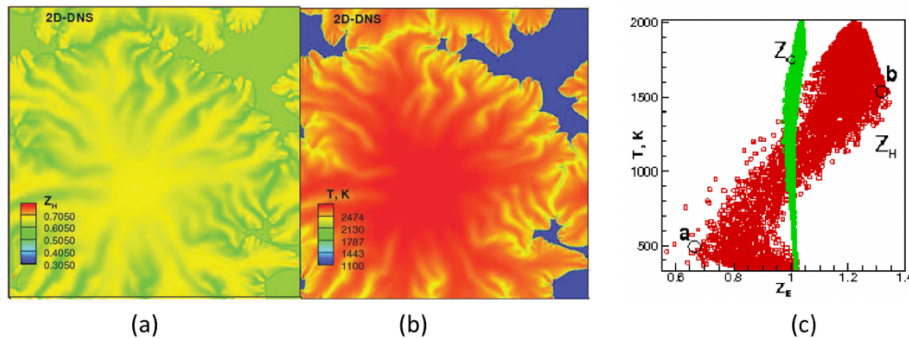

Fig. 6: DNS results of lean hydrogen/air premixed flames at initial temperature 800 K, pressure 30 bar, and equivalence ratio 0.6. (a) 2D field of H element mass fraction, (b) 2D field of temperature, (c) Distribution of physical cells in CCM phase space [26].

This process establishes an efficient and highly precise mapping procedure between physical space and the chemistry phase space, where the chemical reaction rates are integrated. Each cell in the phase space corresponds to several different CFD cells in the physical domain, eliminating the need to perform integration of the chemical reaction rates and heat release in every physical cell. This significantly accelerates computation. The results obtained in the phase space are subsequently mapped back to the physical cells, where they are integrated into

the flow transport terms. This approach substantially reduces computational costs by grouping physical cells into a much smaller number of phase space cells.

The choice of phase space principal variables depends on the flame modes and the fuel. For lean premixed hydrogen/air flames exhibiting significant diffusional thermal instability, characterized by the onset of cellular flame structures as depicted in Fig. 6(a,b), it is found that the phase space variables can be temperature and the mass fraction of element H (J_H). Here, temperature signifies the reaction progress, while J_H represents the fuel stratification resulting from differential diffusion.

For diesel spray combustion, the principal variables in phase space include temperature, the mass fraction of element H (J_H), and the mixing rate, represented by the scalar product of the gradient of J_H [28]. The latter is proportional to the scalar dissipation rate (SDR). In studies involving diesel spray combustion with multiple injections, four principal variables were proposed [29]: temperature (T), equivalence ratio (φ), scalar dissipation rate (χ), and fuel mass fraction (Y_{fuel}). Temperature (T) and fuel mass fraction (Y_{fuel}) are utilized to describe the reaction progress in the high-temperature reaction and low-temperature reaction stages, respectively. Diesel fuel, often modeled using n-heptane, decomposes at low temperatures into heptyl radicals and heptyl peroxides, during which no significant temperature change occurs. Thus, two reaction progress variables are necessary. The equivalence ratio (φ) is employed to depict the fuel stratification in the mixture, while the scalar dissipation rate (χ) describes the mixing rate. The fuel mass fraction (Y_{fuel}) is utilized to model the low-temperature reactions of the diesel surrogate n-heptane.

For the complex multi-mode dual-fuel ammonia/diesel combustion process, a set of phase space variables needs to be developed and evaluated. A more comprehensive set of principal variables has been considered:

- Principal variables relevant to diesel spray combustion, as outlined by Hadapour et al. [29], including temperature (T), equivalence ratio (φ), scalar dissipation rate (χ), and fuel mass fraction Y_{C7H16}.
- Principal variables addressing differential diffusion, such as J_H. In ammonia combustion, where hydrogen concentration may be high, the impact of differential diffusion can be significant.
- Principal variable accounting for the combustion of ammonia in regions where diesel is not present, namely, the mass fraction of NH3, Y_{NH3}.

A more detailed description of the CCM approach can be found in Jangi et al. [26, 27]. The evaluation of phase space principal variables in the application of the CCM approach to ammonia/diesel RCCI engines is presented in Section 3.2, while for DDFS engines, it is discussed in Section 3.3.

3.2. CCM for RCCI engine combustion

A four-stroke ammonia/diesel RCCI engine, studied experimentally [30], is utilized to evaluate the CCM approach. The test engine was a single-cylinder diesel engine system modified from a four-cylinder diesel engine. While three cylinders of the engine operated at fixed speeds and loads, the remaining cylinder, equipped with an independent fuel injection system, intake, and exhaust system, served as the test engine and supported a more flexible combustion mode. NH3 was injected into the intake pipe and mixed with air during intake strokes. Figure 7 illustrates the engine experimental rig, and the table displays the key engine parameters.

Table 3 presents the computational cases. The engine load is 10 bar IMEP, with the ammonia energy share at approximately 60%. The ammonia/air equivalence ratio stands at about 0.47, and the overall equivalence ratio (including both ammonia and diesel) ranges from 0.7 to 0.8. Diesel injection timing varied from -20 to -10 degrees Crank Angle (CA) before Top Dead Center (TDC), with an injection duration of approximately 6 degrees CA.

Displacement (cm³)	1325
Stroke (mm)	130
Bore (mm)	114
Connecting rod (mm)	216
Compression Ratio	18:1
Number of valves	4
Swirl ratio	2.1
IVC (° CA ATDC)	-145
EVO (° CA ATDC)	112
Injector type	Solenoid
Number of nozzles	7
Nozzle hole diameter (mm)	0.175
Spray included angle (°)	155

Fig. 7: Engine experimental rig and key parameters [30].

Table 3. Computational cases

Case	Load (bar)	EP	Φ_{pre}	Φ_g	Fuel mass (mg/cycles)		Pilot SOI (°CA)	Duration °CA
					NH3	Diesel		
1		61.46%	0.483	0.778	94.4	25.8	-20	6.111
2	10bar	60.29%	0.466	0.794	92.9	26.7	-15	6.246
3		58.70%	0.471	0.712	95.1	29.1	-10	6.633

The simulations were conducted utilizing an in-house solver developed on the OpenFOAM V7 platform, as described in [31]. To maintain mesh quality (size and shape of cells) and density throughout the simulation, a novel mesh algorithm was implemented, involving the addition and removal of mesh layers based on the motion of the piston [32]. Simulations were executed using the Reynolds-Averaged Navier–Stokes (RANS) model, selected due to its high computational efficiency required for exploring a wider parameter space [31]. The process of fuel spray was modeled utilizing the well-established Lagrangian–Eulerian approach. The Eulerian system of equations was used to treat the continuum gas phase, while the discrete liquid phase parcel was treated in the Lagrangian framework. The spray droplets underwent distinct processes from injection to vaporization, each simulated with specific submodels, including the KH-RT break-up model [33], Ranz–Marshall correlations heat transfer model [34], Spalding evaporation model [35], trajectory collision model [36], and spray/wall interaction model [37]. A detailed description of the sub-models can be found in our previous work [31]. The chemical kinetic mechanism employed is from Xu et al. [23].

The CCM principal variables discussed in Section 3.1, i.e., temperature (T), equivalence ratio (φ), scalar dissipation rate (χ), mass fraction of element H (J_H), and mass fractions of n-heptane (Y_{C7H16}) and ammonia (Y_{NH3}), show excellent accuracy and speedup rate. Figure 8 shows the comparison of incylinder pressure and apparent heat release rate for the three cases listed in

Table 3. The results from CCM agree very well with the results from direct integration (DI) of the chemical reaction rates without the use of CCM. The CCM results were obtained using a phase space resolution of 100-200 cells in each of the principal variables. It is noted that the not all phase space cells correspond to physical space points, which means that integration of the chemical reaction rates are done only in a small fraction of the phase space cells. Thus, the CCM efficiency is high and insensitive to the number of principal variables.
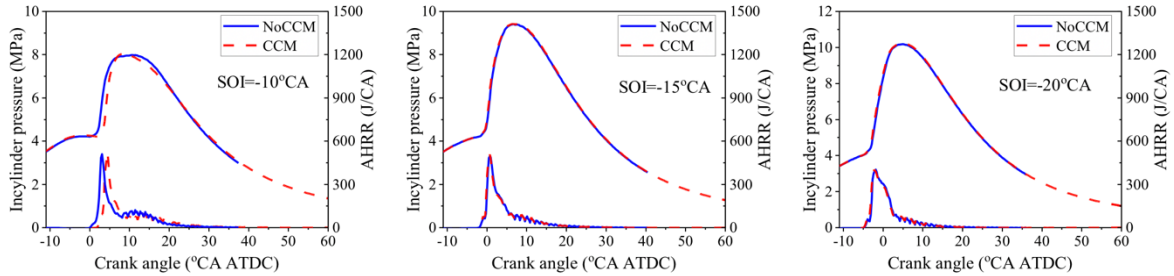

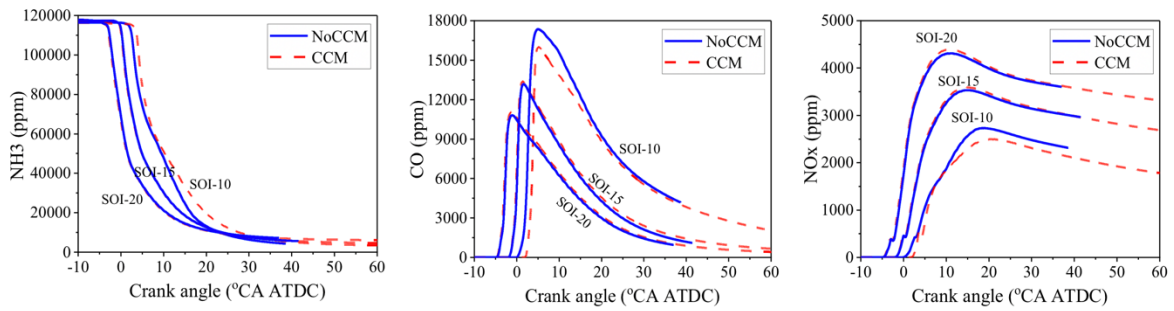Fig. 8: Comparison of incylinder pressure for the three cases listed in Table 3.

Fig. 9: Engine experimental rig and key parameters [30].

Table 4. CCM speedup rate.

Case	Simulation duration	CCM running time (s)	DI running time (s)	Speed up rate
SOI-10	-17 ~ 40 CA	45783	149460	3.27
SOI-15	-17 ~ 40 CA	41843	148200	3.54
SOI-20	-17 ~ 38 CA	43680	149160	3.41

Figure 9 shows a comparison of the incylinder averaged mass fractions of unburned NH3, CO, and NOx at different piston positions around TDC. As the diesel injection is delayed, the ammonia combustion was delayed, the peak CO mass fraction in the cylinder increased, and the peak NOx mass fraction in the cylinder decreased. The engine-out emissions of ammonia is insensitive to the diesel injection timing, but the CO and NOx emissions are sensitive to the diesel injection timing. The CCM results agree very with the DI results without utilizing CCM.

Table 4 shows the computational time used for the computation of the combustion phase, i.e., the piston position in the range of -17 CA aTDC to 40 CA aTDC. The computational time used for the DI simulation is $3.27 - 3.54$ times of that needed for the CCM, demonstrating an excellent speedup rate.

3.3. CCM for DDFS engine combustion

A two-stroke ammonia/diesel DDFS engine was investigated to evaluate the performance of CCM. The engine was studied experimentally [38]. The engine features a bore of 150 mm, a stroke of 225 mm, and a displacement volume of 3.97 L. Operating with a compression ratio of 13.8, the engine runs at a speed of 375 rpm. Both diesel and ammonia are injected directly into the cylinder, with injection pressures set at 65 MPa for ammonia and 100 MPa for diesel. Various injection timings for diesel and ammonia were tested, as listed in Table 5. Four cases were simulated to assess the performance of CCM:

- Case 1: Pure diesel operation (without ammonia injection)
- Case 2: Ammonia injection at SOI_{NH3}=-8 CA ATDC, with an injection duration of 4 ms (resulting in an injected mass of 81.4 mg/cycle)
- Case 3: Ammonia injection at SOI_{NH3}=-8 CA ATDC, with an injection duration of 5 ms (resulting in an injected mass of 103.7 mg/cycle)
- Case 4: Ammonia injection at SOI_{NH3}=-16 CA ATDC, with an injection duration of 5 ms (resulting in an injected mass of 103.7 mg/cycle)

In all cases, diesel injection occurs at SOI_D=-8 CA ATDC, with an injected mass of 43.1 mg per cycle (injection duration of 0.8 ms).

Table 5. Engine operating conditions [38]

|			
Diesel injection timing (°CA ATDC)	−8	−8	−12, −10, −8, −6
Diesel injection quantityper cycle (mg)	43.1	87.2, 43.1	43.1, 87.2
Ammonia injection timing (°CA ATDC)	−8	−16, −8, 0	−8
Ammonia injection signal pulse (ms)	0, 3, 4, 5	5	5
Corresponding crank angle (deg)	0, 6.75, 9, 11.25	11.25	11.25
Ammonia injection quantityper cycle (mg)	0, 62.3, 81.4, 103.7	0, 103.7	0, 103.7
Ammonia injection quantityequivalent diesel (mg)	0, 27.1, 35.4, 45.1	0, 45.1	0, 45.1
Air fuel ratio(λ)	3.8, 3.4, 3.1	3.1	3.1
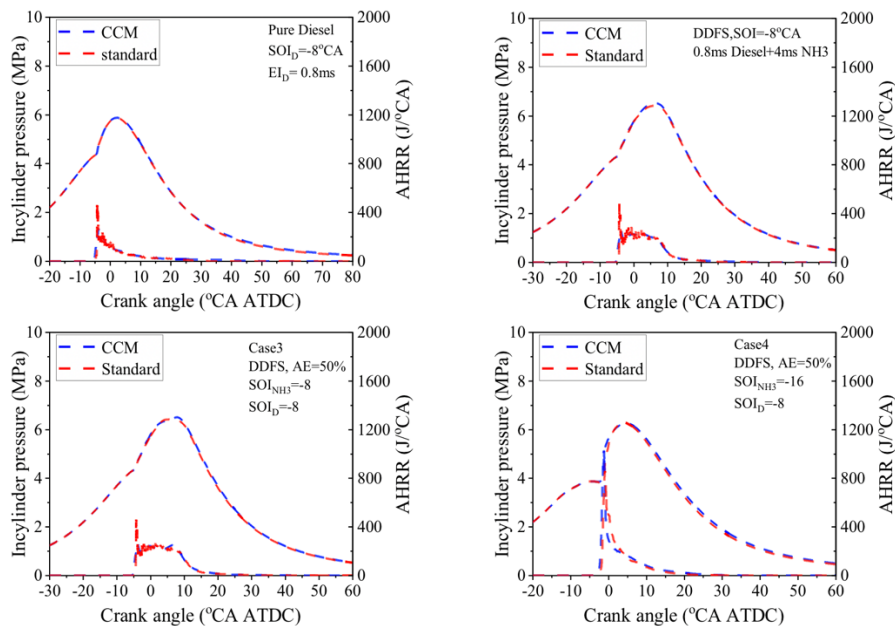
Fig. 10: Comparison of incylinder pressure and apparent heat release rate (AHRR) predicted using RANS and CCM method and the standard direct integration method without the use of CCM.

Fig. 11: Comparison of incylinder NO mass fraction (cylinder mass averaged) predicted using RANS and CCM method and the standard direct integration method without the use of CCM.
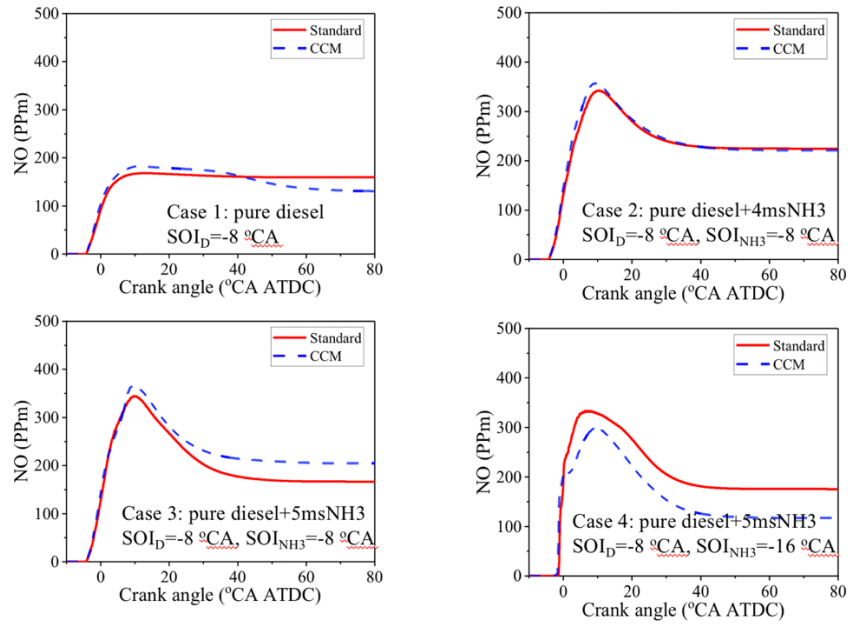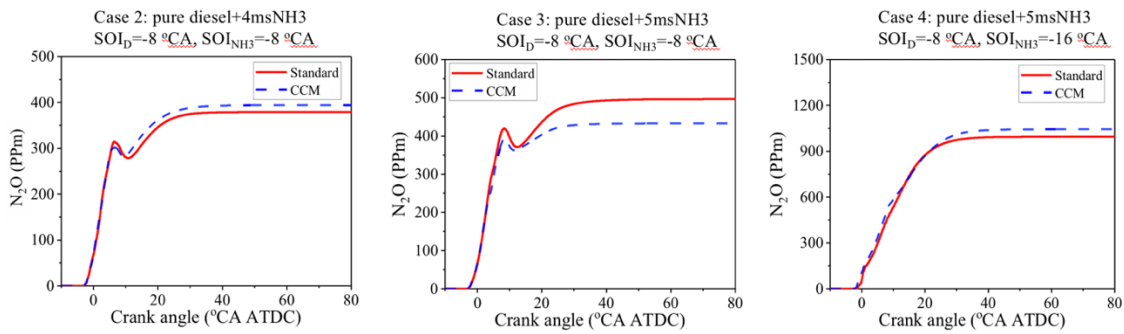

Fig. 12: Comparison of incylinder N_2O mass fraction (cylinder mass averaged) predicted using RANS and CCM method and the standard direct integration method without the use of CCM.

Table 6. Computational time and speedup rate of CCM for Case 2.

CAD	Combustion stage	CPU time, CCM (hours)	CPU time, DI (hours)	Speedup rate
-5 CA ATDC	Diesel ignition	9	26.4	2.93
20 CA ATDC	End of combustion	31.2	54	1.73

The flow, spray, and combustion sub-models remain consistent with those outlined in Section 3.2. A comprehensive description of these sub-models can be found in our previous work [31]. The CFD mesh size averages 1.25 mm, comprising 168 thousand cells at IVC and 1 million cells at -95 degrees CA ATDC.

Figure 10 depicts the pressure in the cylinder and the apparent heat release rate of the charge. Diesel injection commences at -8 CA ATDC, with the onset of diesel ignition indicated by the AHRR peak around -5 CA ATDC. The combustion concludes around 20 CA ATDC. It is evident that the in-cylinder pressure and AHRR profiles from the CCM and the standard direct integration method of reaction rates exhibit good agreement with each other.

Figures 11 and 12 display the in-cylinder mass-averaged NO for the four cases and N2O for the three dual-fuel cases. The pure diesel case (Case 1) exhibits negligible N2O emissions; hence, the results are not presented. The NO and N2O results from CCM closely match those from the method employing direct integration of reaction rates.

Additionally, the computational time required for CCM is significantly lower than that for direct integration of reaction rates, as shown in Table 6. Following the onset of diesel ignition, the speedup rate is 2.93, and by the end of the combustion stage, the speedup rate is 1.73.

4. Conclusion and Future Plans

A novel FGM model was proposed to simulate ammonia/diesel combustion under RCCI engine conditions, employing detailed chemical kinetic mechanisms. Specifically, a 1D RCCI configuration was introduced to generate a numerical approximation of the FGM tabulation function. The model underwent validation against DNS results for two different conditions, demonstrating a remarkable level of agreement in various combustion properties such as ignition delay, flame propagation, fuel consumption, and emission distributions, all achieved within a much shorter simulation time. The new FGM model successfully captures challenging multiple modes and fine-detailed reaction zone structures. Further optimization of the model is possible, particularly for the reaction progress variables, and to accommodate non-unity Lewis number effects in the transport equation of the progress variable.

For CFD simulations using a method directly coupling chemical reaction rates based on reduced kinetic mechanisms, a chemistry coordinate mapping (CCM) method was extended for diesel/ammonia dual-fuel engines. The principal variables were optimized and validated for two types of dual-fuel engines: reactivity controlled compression ignition (RCCI) employing port-injection of ammonia and direct injection of diesel, and DDFS (double direct fuel stratification), where both ammonia and diesel are directly injected into the cylinder close to TDC. For both engine types, results from CCM closely aligned with those from direct integration of chemical reaction rates (without CCM). Utilizing CCM significantly reduced computational time, with a speedup rate about 3.5 for RCCI engines and 1.7 to 2.9 for DDFS engines.

Future application and validation of the CCM method will be conducted for the diesel/ammonia DDFS engine of MAN when experiments are carried out within the ENGIMMONIA consortium.

References

[1] Wartsila, Wartsila ammonia online event, https://www.wartsila.com/marine/, accessed: 2023-12-04 (2023).

[2] L. Xu, S. Xu, X.-S. Bai, J. A. Repo, S. Hautala, J. Hyvonen, Performance and emission characteristics of an ammonia/diesel dual-fuel marine engine, Renew. Sust. Energ. Rev. 185 (2023) 113631.

[3] L. Xu, X.-S. Bai, Numerical investigation of engine performance and emission characteristics of an ammonia/hydrogen/n-heptane engine under RCCI operating conditions, Flow Turbul. Combust. (2023) 1–18.

[4] Z. Zhang, W. Long, P. Dong, H. Tian, J. Tian, B. Li, Y. Wang, Performance characteristics of a two-stroke low speed engine applying ammonia/diesel dual direct injection strategy, Fuel 332 (2023) 126086.

[5] D. Makowski, N2O increasing faster than expected, Nat. Clim. Change 9 (12) (2019) 909–910.

[6] A. Yousefi, H. Guo, S. Dev, S. Lafrance, B. Liko, A study on split diesel injection on thermal efficiency and emissions of an ammonia/diesel dual-fuel engine, Fuel 316 (2022) 123412.

[7] Y. Li, M. Jia, L. Xu, X.-S. Bai, Multiple-objective optimization of methanol/diesel dual-fuel engine at low loads: A comparison of reactivity controlled compression ignition (RCCI) and direct dual fuel stratification (DDFS) strategies, Fuel 262 (2020) 116673.

[8] M. B. Luong, G. H. Yu, S. H. Chung, C. S. Yoo, Ignition of a lean PRF/air mixture under RCCI/SCCI conditions: A comparative DNS study, P. Combust. Inst. 36 (3) (2017) 3623–3631.

[9] X. Zhang, C. Yuan, L. Zhou, W. Zhao, Z. Liu, H. Wei, Effects of initial temperature on ignition and flame propagation of dual-fuel mixture inmixing layer, Combust. Flame 225 (2021) 468–484.

[10] A. Bhagatwala, R. Sankaran, S. Kokjohn, J. H. Chen, Numerical investigation of spontaneous flame propagation under ECCI conditions, Combust. Flame 162 (9) (2015) 3412–3426.

[11] B. Tekgul, H. Kahila, O. Kaario, V. Vuorinen, Large eddy simulation of dual-fuel spray ignition at different ambient temperatures, Combust. Flame 215 (2020) 51–65.

[12] H. Bao, J. Han, Y. Zhang, A. Di Matteo, D. Roekaerts, J. Van Oijen, B. Somers, Large-eddy simulation of dual-fuel spray ignition at varying levels of methane diluted ambient oxidizer using FGM, Fuel 351 (2023) 128901.

[13] H. Bao, N. Maes, H. Y. Akargun, B. Somers, Large eddy simulation of cavitation effects on reacting spray flames using FGM and a new dispersion model with multiple realizations, Combust. Flame 236 (2022) 111764.

[14] L. Xu, Y. Zhang, Q. Tang, B. Johansson, M. Yao, X.-S. Bai, LES/FGM investigation of ignition and flame structure in a gasoline partially premixed combustion engine, P. Combust. Inst. 39 (4) (2023) 4851–4860.

[15] Y. Zhang, S. Xu, S. Zhong, X.-S. Bai, H. Wang, M. Yao, Large eddy simulation of spray combustion using flamelet generated manifolds combined with artificial neural networks, Energy and AI 2 (2020) 100021.

[16] J. Van Oijen, A. Donini, R. Bastiaans, J. ten Thije Boonkkamp, L. De Goey, State-of-the-art in premixed combustion modeling using flamelet generated manifolds, Prog. Energ. Combust. 57 (2016) 30–74.

[17] A. Hadadpour, S. Xu, Y. Zhang, X.-S. Bai, M. Jangi, An extended FGM model with transported PDF for LES of spray combustion, P. Combust. Inst. 39 (4) (2023) 4889–4898.

[18] L. Xu, S. Xu, X. Lu, M. Jia, X.-S. Bai, Large eddy simulation of spray and combustion characteristics of biodiesel and biodiesel/butanol blend fuels in internal combustion engines, Applications in Energy and Combustion Science 16 (2023) 100197.

[19] B. Akkurt, Modelling multi-pulse diesel injection with flamelet generated manifolds, PhD thesis, Technical University of Eindhoven, Eindhoven, Netherlands (2019).

[20] J. Van Oijen, L. De Goey, A numerical study of confined triple flames using a flamelet-generated manifold, Combust. Theor. Model. 8 (1) (2004) 141.

[21] S. Zhong, F. Zhang, M. Jangi, X.-S. Bai, M. Yao, Z. Peng, Structure and propagation of n-heptane/air premixed flame in low temperature ignition regime, Applied Energy 275 (2020) 115320.

[22] N. Zhang, F. Zhang, S. Zhong, Z. Peng, J. Yu, H. Liu, C. Xu, Numerical and theoretical investigation of ethanol/air flame instability, Combust. Theor. Model. 24 (6) (2020) 1108–1129.

[23] L. Xu, Y. Chang, M. Treacy, Y. Zhou, M. Jia, X.-S. Bai, A skeletal chemical kinetic mechanism for ammonia/n-heptane combustion, Fuel 331 (2023) 125830.

[24] A. Krisman, E. R. Hawkes, J. H. Chen, A parametric study of ignition dynamics at ECN spray a thermochemical conditions using 2D DNS, P. Combust. Inst. 37 (4) 113 (2019) 4787–4795.

[25] R. Yu, X.-S. Bai, A. N. Lipatnikov, A direct numerical simulation study of interface propagation in homogeneous turbulence, J. Fluid. Mech. 772 (2015) 127–164.

[26] M. Jangi, R. Yu, X.S. Bai, A multi-zone chemistry mapping approach for direct numerical simulation of auto-ignition and flame propagation in a constant volume enclosure, Combust. Theory Modelling 16:2 (2012) 221-249.

[27] M. Jangi, X.S. Bai, Multidimensional chemistry coordinate mapping approach for combustion modeling with finite rate chemistry, Combust. Theory Modelling 16:6 (2012) 1109-1132.

[28] M. Jangi, T. Lucchini, G. D'Errico, X.S. Bai, Effects of EGR on the structure and emissions of diesel combustion, Proc. Combust. Inst. 34 (2013) 3091-3098.

[29] A. Hadapour, M. Jangi, K.M Pang, X.S. Bai, The role of a split injection strategy in the mixture formation and combustion of diesel spray: A large-eddy simulation, Proc. Combust. Inst. 37 (2019) 4709-4716.

[30] L. Zheng, S. Mi, H. Li, X. Tan, Y. Qian, M. Feng, X. Lu, Experimental study on the combustion and emission characteristics of ammonia/diesel dual fuel engine under high ammonia energy ratio conditions, Journal of the Energy Institute, https://doi.org/10.1016/j.joei.2024.101557

[31] L. Xu, S. Xu, X.-S. Bai, J. A. Repo, S. Hautala, J. Hyvönen, Performance and emission characteristics of an ammonia/diesel dual-fuel marine engine, Renewable and Sustainable Energy Reviews 185 (2023) 113631.

[32] L. Xu, Zhang Y, Tang Q, Johansson B, Yao M, Bai X-S. LES/FGM investigation of ignition and flame structure in a gasoline partially premixed combustion engine. Proc Combust Inst 39 (4), 4851-4860, 2023.

[33] Reitz R, et al. Modeling atomization processes in high-pressure vaporizing sprays. At Spray Technol 1987;3(4):309–37.

[34] Ranz W, Marshall W, et al. Evaporation from drops: Part 2. Chem Eng Progr 1952;48(4):173–80.

[35] Spalding DB. The combustion of liquid fuels. In: Symposium (international) on combustion, Vol. 4. 1953, p. 847–64.

[36] Nordin P. Complex chemistry modeling of diesel spray combustion. Chalmers University of Technology; 2001.

[37] Zhang Y, Jia M, Liu H, Xie M, Wang T, Zhou L. Development of a new spray/wall interaction model for diesel spray under PCCI-engine relevant conditions. At Sprays 2014;24(1):41–80.

[38] Zhang Z, Long W, Dong P, Tian H, Tian J, Li B, Wang Y. Performance characteristics of a two-stroke low speed engine applying ammonia/diesel dual direct injection strategy. Fuel. 2023 Jan 15;332:126086.